

Nanoscale

Accepted Manuscript

This article can be cited before page numbers have been issued, to do this please use: U. B. R. Thumu, M. Bootharaju and T. Pradeep, *Nanoscale*, 2013, DOI: 10.1039/C3NR03463A.



This is an *Accepted Manuscript*, which has been through the RSC Publishing peer review process and has been accepted for publication.

Accepted Manuscripts are published online shortly after acceptance, which is prior to technical editing, formatting and proof reading. This free service from RSC Publishing allows authors to make their results available to the community, in citable form, before publication of the edited article. This *Accepted Manuscript* will be replaced by the edited and formatted *Advance Article* as soon as this is available.

To cite this manuscript please use its permanent Digital Object Identifier (DOI®), which is identical for all formats of publication.

More information about *Accepted Manuscripts* can be found in the [Information for Authors](#).

Please note that technical editing may introduce minor changes to the text and/or graphics contained in the manuscript submitted by the author(s) which may alter content, and that the standard [Terms & Conditions](#) and the [ethical guidelines](#) that apply to the journal are still applicable. In no event shall the RSC be held responsible for any errors or omissions in these *Accepted Manuscript* manuscripts or any consequences arising from the use of any information contained in them.

Thiolate-protected Ag₃₂ clusters: Mass spectral studies of composition and insights into the Ag-thiolate structure from NMR

T. Udayabhaskararao, M. S. Bootharaju and T. Pradeep*

DST Unit of Nanoscience (DST UNS) and Thematic Unit of Excellence (TUE),
Department of Chemistry, Indian Institute of Technology Madras, Chennai-600
036, India. *E-mail:Pradeep@iitm.ac.in

Abstract

Clusters composed of 32 silver atom core, protected with thiolates of glutathione (GSH) and N-(2-mercaptopropionyl)glycine (MPGH) were synthesized by a solid-state route in milligram scale. They do not exhibit surface plasmon resonance unlike their larger sized nanoparticle analogues but show molecule-like features in absorption and luminescence spectra, falling in the visible window. The compositions, Ag₃₂SG₁₉ (SG-thiolate of glutathione) and Ag₃₂MPG₁₉ (MPG-thiolate of MPGH) were understood from electrospray ionization mass spectrometry (ESI MS). Matrix-assisted laser desorption/ionization mass spectrometry (MALDI MS) was not successful for –SG protected clusters as reported before but for Ag₃₂MPG₁₉, a peak at 6.1 kDa

was seen due to fragmentation of the cluster and systematic losses of Ag_2S were observed which increase with increase in laser intensity. Further confirmation of the composition, $\text{Ag}_{32}\text{SG}_{19}$ was made using various studies such as XPS and EDAX. One-dimensional (1D) and two-dimensional (2D) NMR spectroscopic investigations of $\text{Ag}_{32}\text{SG}_{19}$ provided interesting spectral features which indicated the dominant $-\text{[SR-Ag-SR]}-$ structural motif. This structural motif as the predominant entity is found for the first time in silver clusters.

Introduction

Quantum clusters (QCs) of noble metals are molecules composed of a few to hundred metal atom core – even more in some cases, protected with ligands, especially thiols and are fundamentally different from their bulk and plasmonic analogues in terms of their optical, electronic, and structural properties.¹⁻⁴ In the initial years of study, a mixture of gold QCs with unknown compositions were synthesized by the reduction of Au^{3+} in presence of glutathione (GSH, the thiolate form is written as SG).⁵ These clusters were isolated using the technique of gel electrophoresis and their spectroscopic properties were examined in detail. Molecular formulae of these clusters were later understood as $\text{Au}_{10}\text{SG}_{10}$, $\text{Au}_{15}\text{SG}_{13}$, $\text{Au}_{18}\text{SG}_{14}$, $\text{Au}_{22}\text{SG}_{16}$, $\text{Au}_{22}\text{SG}_{17}$, $\text{Au}_{25}\text{SG}_{18}$, $\text{Au}_{29}\text{SG}_{20}$, $\text{Au}_{33}\text{SG}_{22}$ and $\text{Au}_{39}\text{SG}_{24}$ using mass spectral studies.⁶ Subsequently, several new protocols were developed to synthesize these QCs individually i.e. well-defined monodisperse Au_nSR_m .⁷⁻¹¹ Depending on the synthesis conditions, type of protecting ligand, solvent polarity and strength of reducing agent, various monodisperse clusters such as $\text{Au}_{25}\text{SR}_{18}$, $\text{Au}_{38}\text{SR}_{24}$ and $\text{Au}_{144}\text{SR}_{60}$ were synthesized.¹² Size exclusion chromatography was used to detect some of the less prominent clusters such as $\text{Au}_{40}\text{SR}_{24}$ and $\text{Au}_{55}\text{SR}_{30,31}$.¹³⁻¹⁵ In addition to them, Au_{19} ,¹⁶ Au_{18} ¹⁰ and Au_{20} ¹⁷ were also synthesized by controlling kinetics of the

reaction through a slow reduction process. Availability of clusters with known composition, especially crystallization of some of them ($\text{Au}_{25}\text{SR}_{18}$,^{18,19} $\text{Au}_{38}\text{SR}_{24}$,²⁰ $\text{Au}_{36}\text{SR}_{24}$ ²¹ and $\text{Au}_{102}\text{SR}_{44}$ ²²) helped to understand them in greater detail. But corresponding developments have not happened in silver clusters. Although several QCs of silver with known chemical composition such as water soluble Ag_7 ,²³ $\text{Ag}_{7,8}$,²⁴ and Ag_9 ,²⁵ as well as organic soluble $\sim\text{Ag}_{140}$ ²⁶ and Ag_{280} ²⁷ have been made, the growth of the area is not comparable to that of gold analogues. Recently, there has been rapid progress in this area due to the single crystal analysis of Ag_{14} ,²⁸ Ag_{16} ²⁹ and Ag_{32} ²⁹ protected by the combined use of thiolate and phosphine ligands. Analogous to the thiol-protected clusters, they also possess molecule-like behaviour in their optical properties but systematic changes in these properties were not seen due to size and structural differences in cores (such as Ag_6^{4+} , Ag_8^{6+} , and Ag_{22}^{12+}). For example, while Ag_{14} is yellow emissive, Ag_{16} and Ag_{32} exhibit blue emission. Their structures are interesting and provide new insights into the atomic structure of thiolated-Ag QCs in comparison to Au QCs.

In recent years, a variety of methods have been developed to produce stable thiolate-protected silver QCs. Among them is the synthesis through a solid-state route.²⁵ The time required to produce the desired cluster is substantially less here. High yield of clusters and easy handling of the reaction made this route novel. It is expected that this protocol opens up a new way for the synthesis of a variety of cluster materials. For example, by varying precursor ratios, reducing agents, temperature and solvents, numerous cluster materials are produced through this route. Here, we report the preparation of thiolated Ag_{32} clusters with two ligands in aqueous phase through this method and their most essential characterization. Assignment of chemical composition was made based on mass spectrometry (MS) including electrospray ionization (ESI) and matrix-assisted laser desorption ionization (MALDI), coupled with elemental analysis and

X-ray photoelectron spectroscopy (XPS). We proposed the Ag-thiolate structure of the cluster based on a detailed nuclear magnetic resonance spectroscopic (NMR) study.

Experimental section

Materials and methods

Chemicals: All the chemicals were commercially available and were used without further purification. Silver nitrate (AgNO_3 , 99%), glutathione (GSH, 97%), N-(2-mercaptopropionyl)glycine (MPGH, Aldrich), acrylamide (AR grade), N,N'-methylenebisacrylamide (BIS) (AR grade), ammonium persulfate and N,N,N',N'-tetramethylethylene diamine (TEMED) were purchased from SRL Chemical Co. Ltd., India. Sodium borohydride (NaBH_4 , 99.99%, Aldrich), ethanol (HPLC grade, 99.9%, Aldrich) and methanol (HPLC grade) were used as received.

Synthesis of $\text{Ag}_{32}\text{SG}_{19}$: About 23 mg of $\text{AgNO}_3(\text{s})$ was added to 200 mg of $\text{GSH}(\text{s})$ at room temperature and the mixture was ground well in a mortar to make $\text{Ag}(\text{I})\text{SG}$ thiolate. About 25 mg $\text{NaBH}_4(\text{s})$ was added and grinding was continued further for 10 more minutes. After that, 10 mL of distilled water was added slowly (in one mL step) which resulted in the formation of a reddish brown solution. Clusters were precipitated immediately by the addition of excess ethanol. The resulting precipitate was collected and washed repeatedly with ethanol through centrifugal precipitation. Finally, precipitate was dried and collected as a reddish brown powder (~ 26 mg). This was termed as crude cluster (CC) in this paper. The dried product was stored in the laboratory atmosphere. Photographs of the synthesis at various stages are shown in Electronic Supplementary Information (ESI), Scheme S1†. The powder was dissolved in water (10 mg/mL)

and kept at ambient conditions overnight. This resulted in color change from reddish brown to pale pinkish red. This was referred to as aged crude clusters (ACC).

Polyacrylamide gel electrophoresis (PAGE): PAGE was performed using previously reported procedure.³⁰ A gel electrophoresis unit with 1 mm thick spacer (Bio-rad, Mini-protein Tetra cell) was used to process the PAGE. The total contents of the acrylamide monomers were 28% (Bis:acrylamide) = 7:93 and 3% (Bis:acrylamide) = 7:93 for the separation and condensation gels, respectively. The eluting buffer consisted of 192 mM glycine and 25 mM tris(hydroxymethylamine). The crude cluster was dissolved in 5% (v/v) glycerol-water solution (1.0 mL) at a concentration of 10 mg/mL. The sample solution (1.0 mL) was loaded onto a 1 mm gel and eluted for 4 h at a constant voltage of 150 V to achieve separation shown in Fig. 1. The gel fractions containing the clusters were cut out, ground, and dipped in ice cold distilled water (2 mL) for 10 min. Subsequently, the solutions were centrifuged at 20,000 rpm for 5 min at -10 °C, followed by filtering with filter paper having 0.22 μm pores to remove the gel lumps suspended in the solution. Separation of cluster 3 was done carefully. For measurements we have cut only the top portion of band 3 (marked in the PAGE photograph) where it is separated far away from the adjacent clusters. Clusters 2&3 are merged only at their boundary. Cluster 2 showed as a separate band which indicates that it was not fully mixed with cluster 3. Further PAGE on cluster 3 shows the same UV-vis, luminescence and ESI MS as that of cluster 3.

Synthesis of Ag₃₂MPG₁₉: About 23 mg of AgNO₃(s) was added to 110 mg of MPGH(s), 1.5 mg of NaOH(s) at room temperature and the mixture was ground well in a mortar to make Ag(I)MPG thiolate. About 25 mg NaBH₄(s) was added and grinding was continued further for

10 more minutes. After that, 10 mL of distilled water was added slowly (in one mL step) which resulted in the formation of a reddish brown solution. Clusters were precipitated immediately by the addition of excess ethanol. The resulting precipitate was collected and washed repeatedly with ethanol through centrifugal precipitation. Finally, precipitate was dried and collected as a reddish brown powder. The powder was dissolved in water (10 mg/mL) and kept at 10 °C overnight. Resultant solution is called as Ag@MPG clusters in the text. Through ESI MS and MALDI MS it is understood the composition of the cluster as Ag₃₂MPG₁₉.

Instrumentation: UV-vis spectra were measured with a PerkinElmer Lambda 25 instrument in the range of 200-1100 nm. Luminescence measurements were carried out on a Jobin Yvon NanoLog instrument. The band pass for excitation and emission was set as 2 nm. Circular dichroism studies were measured using a Jasco Model J-810 circular dichroism spectropolarimeter in the range of 200-800 nm. X-ray photoelectron spectroscopy (XPS) measurements were conducted using an Omicron ESCA Probe spectrometer with polychromatic Mg K α X-rays (hv=1253.6 eV). The samples were spotted as drop-cast films on a sample stub. A constant analyzer energy of 20 eV was used for the measurements. High resolution transmission electron microscopy of clusters was carried out with a JEOL 3010 instrument. The samples were drop casted on carbon-coated copper grids and allowed to dry under ambient conditions. FTIR spectra were measured with a PerkinElmer Spectrum One instrument. KBr crystals were used as the matrix for preparing samples. ¹H NMR were measured with a 500 MHz Bruker Advance III spectrometer operating at 500.13 MHz and equipped with a 5 mm triple-resonance PFG probe. Solutions were made in 99.98% D₂O (Aldrich) and sealed immediately. The signal of the solvent served as the reference for the field-frequency lock. All experiments were performed at a

temperature of 25 °C. Standard Bruker pulse programs (Topspin 2.1) were employed throughout. As PAGE purified samples contain tiny quantities of the gel, ¹HNMR was performed with the aged crude, which was identical to cluster 3. Mass studies were conducted using an electrospray mass spectrometry (ESI MS) system, LTQ XL (Thermo scientific). Samples of 50 ppm concentration, taken in 3:7 water/methanol mixture were electrosprayed. Negative ion spectra showed characteristic features in view of the carboxylate species present. Positive ion spectra did not have distinct molecular ion features. Optimized conditions for the negative ion spectra were: capillary temperature: 150 °C, capillary voltage: -34 V, source voltage: -5.7 kV, tubular lens voltage: -110 V and flow rate: 5 μL/min. Matrix-assisted desorption ionization mass spectrometry (MALDI MS) studies were conducted using a Voyager-DE PRO Biospectrometry Workstation from Applied Biosystems. A pulsed nitrogen laser of 337 nm was used near threshold laser intensity in negative mode. Matrix solution was prepared by dissolving 10 mg of α-Cyano-4-hydroxycinnamic acid (CHCA) matrix in 1:1 mixture of acetonitrile (0.5 mL) and trifluoroacetic acid (0.5 mL, 0.1% in DI water). 2 μL of as-synthesized Ag@MPG clusters in water were uniformly mixed with 5 μL of matrix solution. A volume of 2.5 μL of the cluster-matrix mixture was spotted on the target and allowed to dry at ambient conditions. Scanning electron microscopic (SEM) and energy dispersive X-ray (EDAX) analyses were done in a FEI QUANTA-200 SEM. For measurements, samples were drop casted on an indium tin oxide coated conducting glass and dried in vacuum. Powder XRD patterns of the samples were recorded using PANalytical X'pertPro diffractometer. The powder samples of parent silver nanoparticles and clusters were taken on a glass plate and the X-ray diffractogram was collected from 5 to 100 degrees in 2 theta using Cu Kα radiation.

Results and Discussion

Crude cluster was obtained by grinding the metal precursor and the ligand followed by reduction with $\text{NaBH}_4(\text{s})$. In this process, initially silver thiolate is formed due to the reaction between AgNO_3 and GSH at the interface. High affinity of sulfur to noble metal ions is responsible for thiolate formation which was confirmed from the IR spectrum of the ground mixture, where the S-H_{str} of GSH was absent. Upon addition of sodium borohydride in the solid form, the ground mixture turns to a brownish black powder which shows high affinity to water. At this point, compounds are mixed well, the essential steps of particle formation such as nucleation and growth are controlled due to the lack of protic solvent, which facilitates fast reduction to form metallic particles. This control is important in minimizing the formation of mixture of clusters compared to solution phase synthesis.

The sample, crude cluster (CC) in water shows an absorption profile different from plasmonic nanoparticles. A peak at 480 nm and shoulders at 550 and 350 nm were observed (Fig. S2a†). Silver clusters protected by glutathione and analogous thiols exhibit distinct features in the region of 300-800 nm.^{23-27, 30-38} This product, CC is a mixture of individual silver QCs, as revealed by polyacrylamide gel electrophoresis (PAGE, detailed procedure is in experimental section). Five different bands were separated and are clearly observable on the gel as shown in Fig. 1a. These five bands of different clusters were cut and soaked in ice cold distilled water. Individual clusters were extracted into water, and their distinctive aspects are clearly observable by the appearance of respective colors. Photographs of the five solid gels and the cluster solutions are given in Fig. 1b. Clusters extracted from these bands are referred to as clusters 1-5, corresponding to the band labels in Fig. 1a. Absorption profiles of all the clusters in water show

molecule-like behavior (Fig. 1c). Cluster 5 shows a near-IR absorption peak at 750 nm, along with two other peaks at 540 and 415 nm. Cluster 4 shows a broad peak centered at 550 nm, along with a small hump at 350 and 640 nm. Cluster 3 shows a sharp peak 480 nm along with a shoulder peak at 610 nm. Cluster 2 shows distinct peaks at 420, 430 and 490 nm. Cluster 1 shows a broad peak at 490 nm. UV-vis investigations show that band gaps of these clusters vary with core sizes. Blue shift in the HOMO-LUMO gap with decreasing core sizes is observed (traces 5 to 1), as seen in gold⁶ and silver³¹ clusters. The luminescence properties also change in clusters 1-5. Clusters 4 and 5 did not show visible luminescence whereas 2 and 3 exhibit luminescence with maxima at 670 and 680 nm, respectively (Fig. S3†). The shift in luminescence maxima is consistent with the change in cluster size. The yield of CC was ~ 26 mg, starting from 23 mg of AgNO₃. Cluster 3 shows better yield (~ 15 mg from 23 mg of AgNO₃) and stability than the other QCs.

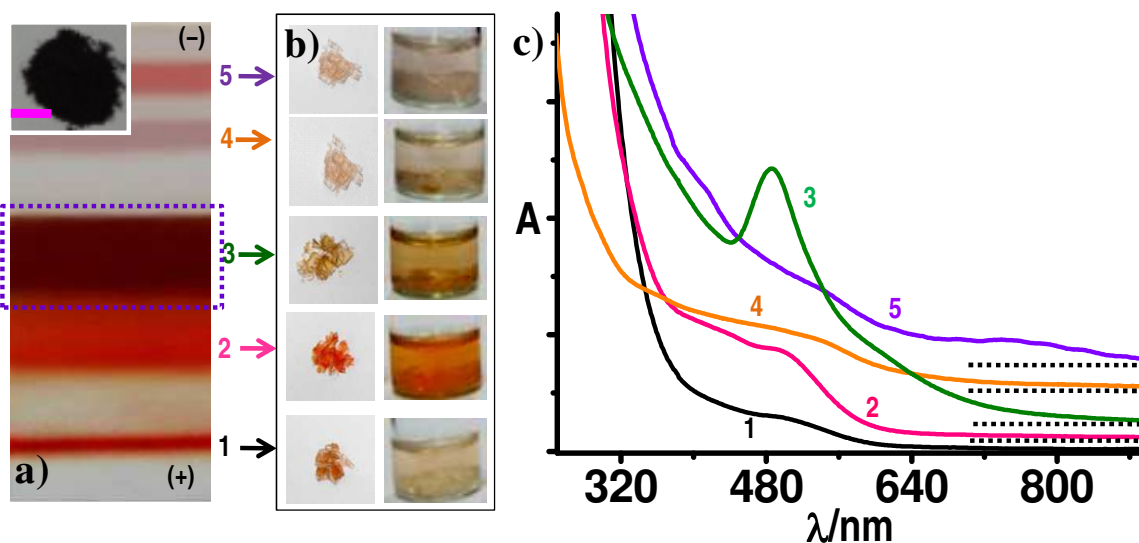


Fig. 1 a) Distinct bands are seen in the gel, derived from the crude cluster (black color powder in inset of a). Scale bar on inset of (a) is 1 cm. b) Photographs of solidified gel fractions of clusters 1-5 (left) and their water extracts (right). c) UV-vis absorption spectra of clusters 1-5 extracted from each band after gel electrophoresis of the crude cluster.

About 10 mg of crude cluster was dissolved in 1.0 mL water and kept at ambient conditions overnight. There was a black precipitate and a clear solution. The precipitate was discarded, which may be due to the decomposition of other metastable clusters. The resultant supernatant is referred to as aged crude cluster (ACC). Aging resulted in a change of color of the solution from reddish brown (CC) to faint pinkish red (ACC) and this change is also reflected in the corresponding powder samples. The powder samples of CC and ACC are black and reddish brown, as shown in insets of Fig. 1a and Fig. 2b, respectively.

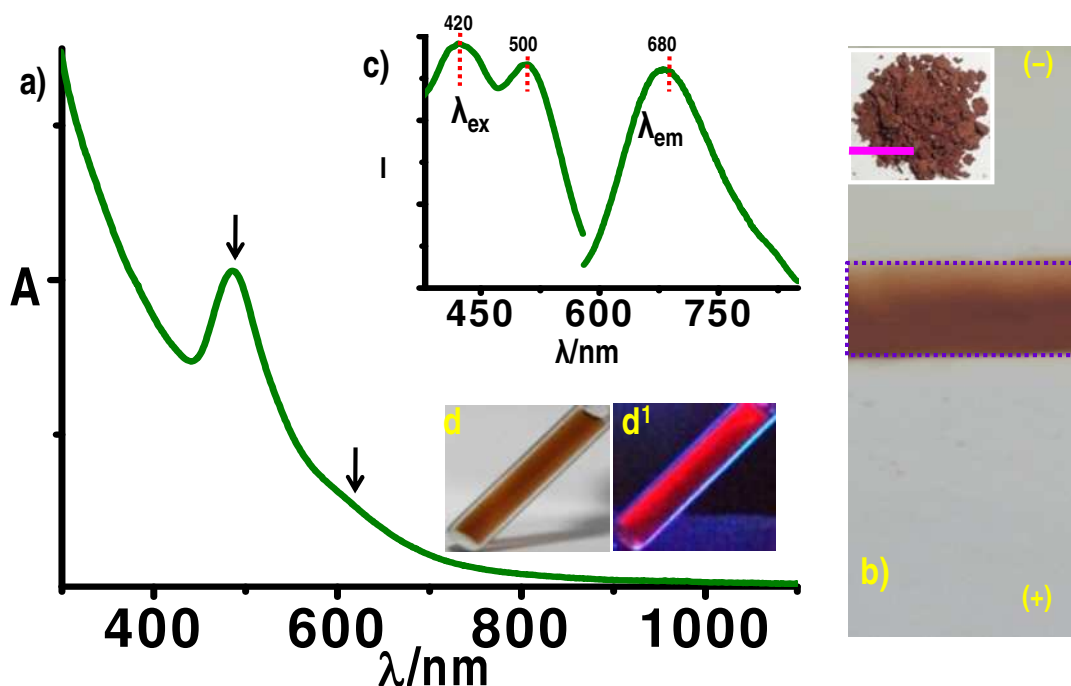


Fig. 2 a) UV-vis absorption spectrum of the sample in (b). Distinct peaks are marked. b) Photograph of the PAGE band derived from aged crude. Inset of (b) is the aged crude cluster in powder form. Scale bars on inset of (b) is 1 cm. (c) Excitation and emission spectra of the same. Photographs of this solution in water collected under visible (d) and UV light (d¹).

The absorption spectra of ACC (Fig. S2b[†]) and cluster 3 (Fig. 1) were similar and therefore, the discarded residue may be due to the decomposition of metastable clusters, 5, 4, 2

and 1. ^1H NMR data also support the conversion of a mixture of clusters to a single cluster as there is a reduction in peak width (see later). Features in the circular dichroism (CD) spectrum of ACC matched with its absorption peaks in the 300-700 nm range (Fig. S4†) with strong Cotton signals due to the intrinsic chiral metal core.^{30,33,35,37} It is also noted that the CD signals are matching with the glutathione protected silver cluster reported by Kitaev *et al.*³⁷ The powder obtained after freeze-drying the ACC solution was subjected to PAGE, which showed the presence of a single band (Fig. 2b) whose absorption and luminescence profiles (Fig. 2a† and inset c, respectively) match perfectly with those of cluster 3 (both the bands, exhibiting the same mobilities are marked with dotted boxes on Fig. 1a & 2b, respectively). Absorption spectral features of cluster 3 and Ag@SG clusters from the literature^{25,31,37} are comparable (Fig. S5†). All of them show similarities in the sharp and shoulder peaks at ~ 480 and ~ 600 nm, respectively. The cluster solution exhibit luminescence in the red region, photographs of the solution under visible and UV light are shown in insets d and d¹, respectively. Interestingly, the absorption spectrum of recently crystallized Ag₃₂ cluster²⁹ also exhibits a strong peak at 485 nm and a weak peak at 600 nm along with few additional structures at 450 and 750 nm; the latter two are absent in our present system. Also the crystallized cluster²⁹ exhibits blue emission but the present system is red emitting. These differences in the optical properties of the systems may be due to the ligand-dependent structural changes. It has to be noted that the ligand, (1,2-bis(diphenylphosphino)ethane (DPPE), useful to join tetrahedrally coordinated shell-Ag atoms of the Ag₂₂¹²⁺ core, are absent in the present system.

The cluster was characterized with various tools as well. As ACC, its PAGE-purified product and cluster 3 gave identical results, the former was used for most of the studies, unless

noted otherwise. The cluster responsible was identified as $\text{Ag}_{32}\text{SG}_{19}$ and the details will be discussed below.

It is worth noting that there are some minor differences in the absorption spectra of ACC and the PAGE-purified product (cluster 3). However, absorption profiles of the PAGE product of ACC (Fig. 2a) and cluster 3 (Fig. 1, trace 3) are the same. An extra peak was observed at 420 nm in ACC (Fig. S2†) and not in the PAGE purified products. Although there is this difference, the excitation and emission spectra for all the clusters are the same (Fig. S3† & Fig. 2c). This difference in the absorption spectrum is due to difference in pH of the solution. Absorption profiles of these clusters show slight changes with pH. The 420 nm peak in ACC at pH 4.2 was absent at pH 6.0. The running gel in electrophoresis is maintained at pH 8.8, and this results in a change in pH after PAGE. Another important aspect to mention is that the 420 nm band of the excitation spectrum of ACC (Fig. 2c) resembles the UV-vis spectrum, indicating that this peak is part of the absorption spectrum and is not due to another cluster. These aspects indicate that they both are the same chemically.

Although crystallography is needed for complete characterization, most of the information on the composition of QCs is available from mass spectrometry.^{4,6} It is also important to note that -SG protected clusters are difficult to crystallize and crystal structure of none of them is available till now. The chemical compositions of -SG protected gold clusters were understood solely based on ESI MS.⁶ Unlike in the case of gold QCs, obtaining quality ESI MS of silver clusters is difficult due to their poor stability. In most cases, the ESI conditions, especially the capillary and transfer tube temperatures cause decomposition of the clusters. As a result, only a few Ag QCs with known composition exist till now. Most of the studies of these clusters are limited to understand their optical properties,^{30,33-37,39} and applications in sensing.⁴⁰⁻⁴²

Negative ion ESI MS of cluster 3 and aged cluster in water:methanol mixture yield the same ESI MS data. The spectra are composed of a series of multiply charged anions originating from deprotonation of the carboxyl moieties of the -SG ligands as it is a dicarboxylic acid. It can undergo two ionizations, but in the pH of the cluster solution (~4.2), a monoanion (SG-H)⁻ is preferred. However, -SG ligand can also exist as a sodium salt and therefore the mono anion formed may be represented as (-SGNa-2H)⁻. As there are multiple SG ligands, there are a number of such species.

Cluster 3 shows a series of peaks in the range of m/z 1200-2500 (Fig. 3). However, it is quite difficult to understand the peaks due to complexity of the spectrum. Recently, Griffith *et al.*⁴³ reported the mass spectrum of Ag₃₂SG₁₉, isolated from gel electrophoresis of crude clusters. Absorption profile of this cluster matches well with our cluster (Fig. S5†). But, the mass spectral series obtained by Griffith *et al.* is different from our study. This discrepancy may be due to the synthesis protocol which adds sodium ions in our case and also due to instrumental variations. The calculated multiply charged peaks for [Ag₃₂(SGNa-2H)₁₉H_{19-q}]^{q-} are matching well with the ESI MS data [Note: Ag₃₂(SGNa-2H)₁₉H_{19-q} is the parent neutral molecule]. For example, a highly intense peak centred at m/z 1941 corresponds to [Ag₃₂(SGNa-2H)₁₉H₁₄]⁵⁻. Upon close observation we find that the peak is composed of four peaks at m/z 1936 [Ag₃₂(SGNa-2H)₁₉H₁₄]⁵⁻, m/z 1941 [Ag₃₂(SGNa-2H)₁₉NaH₁₃]⁵⁻, m/z 1945 [Ag₃₂(SGNa-2H)₁₉Na₂H₁₂]⁵⁻ and m/z 1949 [Ag₃₂(SGNa-2H)₁₉Na₃H₁₁]⁵⁻ (inset i, Fig. 3). Such sodium additions are common in cluster mass spectrometry.^{23,25} Similarly, mass spectral peaks corresponding to [Ag₃₂(SGNa-2H)₁₉H_{19-q}]^{q-} also appeared at the calculated positions, where q is the overall charge of the cluster (6, 7, 8 and 9). For example, the peaks due to [Ag₃₂(SGNa-2H)₁₉H₁₃]⁶⁻, [Ag₃₂(SGNa-2H)₁₉H₁₂]⁷⁻, [Ag₃₂(SGNa-2H)₁₉H₁₁]⁸⁻ and [Ag₃₂(SGNa-2H)₁₉H₁₀]⁹⁻ are at m/z 1617, 1386, 1212, and 1078,

respectively. Although the calculated positions match well, the resolution at these charge states is not adequate to see the isotope pattern of silver. The peaks appeared are quite broad and several other peaks surround the main peak. This complication is due to the presence of sodium adducts. The other complication corresponds to a cleavage of the amide bond between glutamic acid and cysteine, a fragmentation process commonly observed in glutathione, as evidenced by its presence in the tandem mass (mass spectrometry/mass spectrometry, MS/MS) spectrum of glutathione itself (Fig. S6†). This kind of fragmentation is also observed for glutathione protected gold clusters.¹⁰ ESI MS in the range of m/z 400-1200 show low mass region peaks at m/z 936, 828, 522 and 414 assigned to $[\text{Ag}_3\text{SG}_2\text{-H}]^-$, $[\text{Ag}_2\text{SG}_2\text{-H}]^-$, $[\text{Ag}_2\text{SG-H}]^-$ and $[\text{AgSG-H}]^-$, respectively (Fig. S7†). We measured the mass spectra of the well-known cluster, $\text{Au}_{25}\text{SG}_{18}$ under these conditions and the expected spectrum was seen (Fig. S8†), which confirms the accuracy of the data.

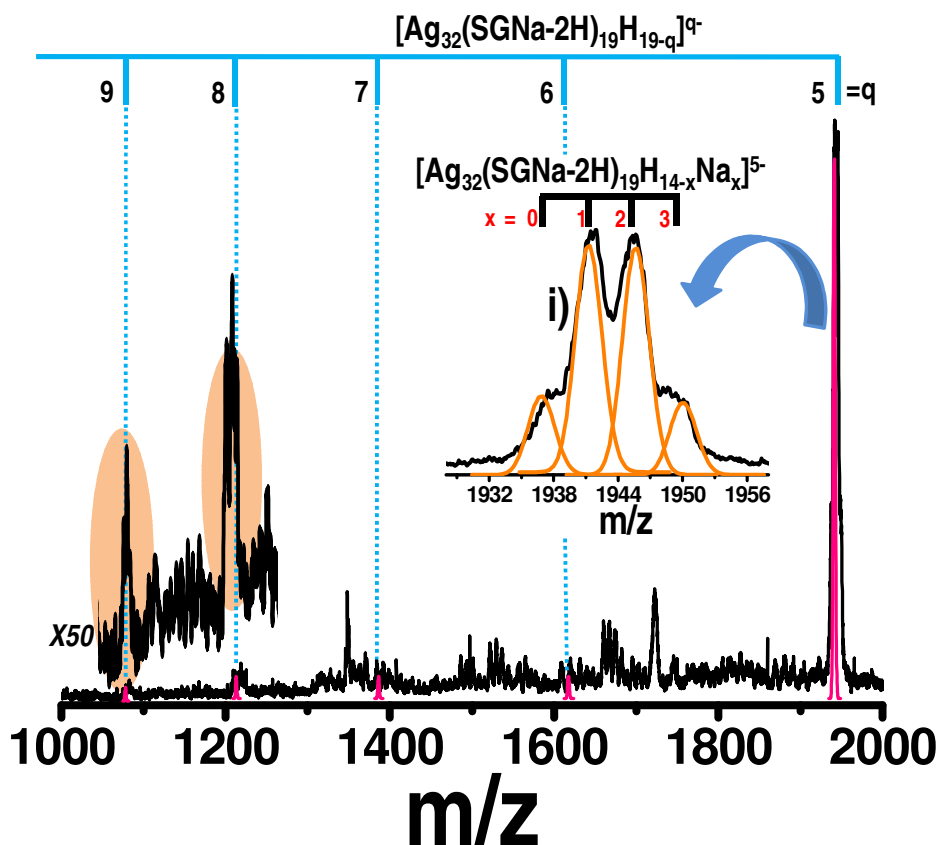


Fig. 3 ESI MS of $\text{Ag}_{32}\text{SG}_{19}$ in negative mode in the range of m/z 1000-2000. Calculated positions corresponding to the multiply charged species (5^- to 9^-) of $[\text{Ag}_{32}(\text{SGNa-2H})_{19}\text{H}_{19-q}]^{q-}$ are shown on the top of the spectrum. Pink colored peaks correspond to the calculated peaks positions of $[\text{Ag}_{32}(\text{SGNa-2H})_{19}\text{H}_{19-q}]^{q-}$. Inset i) Comparison of the calculated and experimental spectra of $[\text{Ag}_{32}(\text{SGNa-2H})_{19}\text{H}_{14-x}\text{Na}_x]^{5-}$, where $x = 0, 1, 2$ and 3 .

In view of the poorly resolved peaks in the ESI MS data, we wanted to have additional information on the composition of the cluster using other methods. The best option is to compare the result with another soft ionization technique. MALDI MS of the cluster was not successful for further confirmation of the assignment. Note that so far there is no report of the MALDI MS of intact clusters protected with glutathione. In order to obtain both MALDI MS and ESI MS, we

tried to synthesize a cluster having the same core with ligands such as cysteine, mercaptosuccinic acid and N-(2-mercaptopropionyl)glycine. Among them, the cluster protected with N-(2-mercaptopropionyl)glycine (MPGH; its thiolate is labeled as MPG) was selected for further study as its absorption profiles matched exactly with cluster 3 ($\text{Ag}_{32}\text{SG}_{19}$). The cluster also gave acceptable MALDI and ESI MS features. We present these data below.

MPG protected Ag QCs (Ag@MPG) were synthesized using the same method used for $\text{Ag}_{32}\text{SG}_{19}$ (see experimental section). Precipitate of clusters was taken in 10 mL distilled water and kept for aging at 10 °C. The pH of the resultant solution was 6.0. It showed a sharp peak at ~ 480 nm and a shoulder around ~ 600 nm in its absorption profile (inset of Fig. 4). At the same pH, $\text{Ag}_{32}\text{SG}_{19}$ also shows the same absorption spectrum. Similarity in absorption profiles of these clusters proves that both are having the same cluster core. In the case of the luminescence spectrum, there is slight shift (10-15 nm) in the emission peak position. Unlike in the case of $\text{Ag}_{32}\text{SG}_{19}$, these clusters do not show visible luminescence under UV light illumination, indicating very low quantum yields compared to glutathione protected ones. It is known that -SG protected Au_{25} shows higher quantum yield compared to other thiols.⁴⁴ It is attributed to the electron donating capability (of -SG) due to the presence of electron rich groups (e.g., carboxylic and amino groups). In the case of MPG, fewer number of electron rich groups made the system to have lower quantum yield. Ag@MPG clusters exhibit a single emission at 700 nm when excited at 470 and 540 nm (Fig. S9[†]). However, there is slight shift in excitation and emission positions of the clusters ($\text{Ag}_{32}\text{SG}_{19}$ and Ag@MPG). Note that ligands play an important role in the luminescence profile.^{8,44}

This cluster was subjected to MALDI MS using CHCA as the matrix. Negative ion mode MALDI MS (Fig. 4) at threshold laser power (~1700) shows a peak maximum at ~6.1 k. No

cluster, other than the species giving the 6.1 k maximum was present in the sample. The peak was quite broad compared to the calculated peak and also in comparison to typical MALDI MS data of Au clusters.

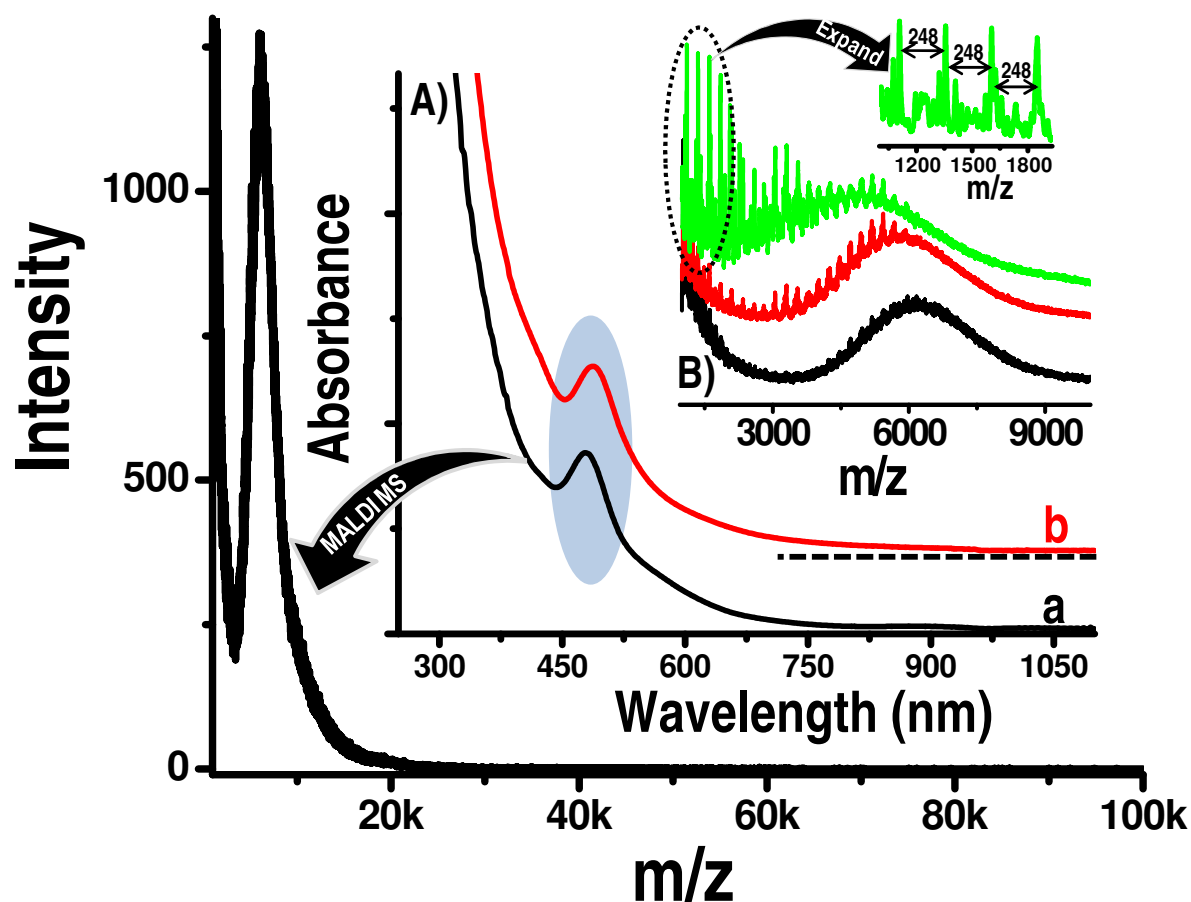


Fig. 4 MALDI MS of Ag@MPG in negative mode. A) UV-vis absorption spectra of Ag@MPG (a) and Ag₃₂SG₁₉ (b) clusters at pH 6.0. B) Laser dependent MALDI MS spectra of the Ag@MPG cluster at near threshold intensity (black trace, ~1700) and at higher laser intensities (red and green traces). Inset of B show the expanded region of MALDI MS in high laser intensity (~3500).

Upon closer observation, the 6.1 k peak is composed of peaks spaced at m/z 248, especially on the left of the peak suggesting progressive loss of Ag₂S. Thus, even at threshold laser intensity, selective fragmentation occurs. The loss of Ag-MPG thiolates is unlikely, which would

have given a much larger spacing of m/z 270. This loss is reflected in the experimentally observed mass spectral position (6.1 k) while the calculated peak position for $\text{Ag}_{32}\text{MPG}_{19}$ is 6.5 k which was confirmed by ESI MS (see below). We conclude that the alkyl chains are partially dissociated (~3 alkyl groups (~0.13 kDa for each); 6.5-6.1 kDa = 0.4 kDa) from the cluster core during ionization, which also explains the increased peak width. Indeed, loss of alkyl chains by carbon-sulfur (C-S) bond cleavage is common in monolayer protected clusters of gold and silver. Peak at 6.1k is increasingly shifted towards the low mass region with increasing laser intensity and the spectrum is dominated by series of peaks separated by m/z 248 due to Ag_2S loss indicating the loss of a major portion of the alkyl chains (inset of Fig. 4B). By the use of a more optimized matrix, this fragmentation may be avoided. It is important to note that an optimized matrix such as Trans-2-[3-(4-tert-butylphenyl)-2-methyl-2-propenylidene]malononitrile (DCTB) is essential for a high quality mass spectrum of $\text{Au}_{25}\text{PET}_{18}$.⁴

$\text{Ag}@MPG$ cluster was also subjected to ESI MS. Fig. 5 shows the negative ion (ESI) mass spectrum of $\text{Ag}@MPG$ clusters in water:methanol mixture. As MPG is a mono carboxylic acid and its ionization by the loss of H^+ results in $(\text{MPG-H})^-$. A series of multiply charged species were observed in the mass spectrum of the cluster due to $[\text{Ag}_{32}(\text{MPG-H})_{19}\text{Na}_x\text{H}_{19-x-q}]^{q-}$, where $q = 3, 4$ and 5 . The multiply charged peaks are quite broad due to the addition of sodium ($x = 8, 9$ and 10). Just as in the case of $-\text{SG}$, half the carboxylate functional groups contain sodium. For example, peak at m/z 2254 (due to the triply charged species) is due to the merger of peaks corresponding to $[\text{Ag}_{32}(\text{MPG-H})_{19}\text{Na}_8\text{H}_8]^{3-}$, $[\text{Ag}_{32}(\text{MPG-H})_{19}\text{Na}_9\text{H}_7]^{3-}$ and $[\text{Ag}_{32}(\text{MPG-H})_{19}\text{Na}_{10}\text{H}_6]^{3-}$ (inset of Fig. 5). However, there is complexity in the data (extra peaks in the spectrum labeled with *) which may be superimposition of other charged species or other possible fragmentations. In order to understand the system in detail, an improved mass spectrum

is required. This is difficult in view of the multiply charged species, although we are continuing our efforts. Peaks of other charges, $[\text{Ag}_{32}(\text{MPG-H})_{19}\text{Na}_8\text{H}_7]^{4-}$ and $[\text{Ag}_{32}(\text{MPG-H})_{19}\text{Na}_8\text{H}_6]^{5-}$ were also seen with good intensity. Even at low capillary temperatures, clusters undergo fragmentation resulting in peaks in the low mass region. These fragment peaks appeared with characteristic mass spacing due to silver isotopes, i.e. m/z 2. These peaks at m/z 1080 and 1188 correspond to $[\text{Ag}_4\text{MPG}_4\text{-H}]^-$ and $[\text{Ag}_5\text{MPG}_4\text{-H}]^-$, respectively. These peaks and their sodium adducts are labeled in Fig. 5. Intense peak at m/z 1902 in the mass spectrum corresponds to the triply charged sodium salt of $\text{Ag}_{27}\text{MPG}_{16}$, derived from the loss of silver thiolates ($[\text{Ag}_5\text{MPG}_3\text{-H}]^-$, which appeared in the low mass region, shown in orange color), from its parent ion, $[\text{Ag}_{32}(\text{MPG-H})_{19}\text{Na}_8\text{H}_8]^{3-}$. Expanded spectrum of $[\text{Ag}_5\text{MPG}_3\text{-H}]^-$ is given in Fig. S10†. Based on the agreement between the experimental and calculated peaks, the composition of Ag@MPG cluster is confirmed as $\text{Ag}_{32}\text{MPG}_{19}$.

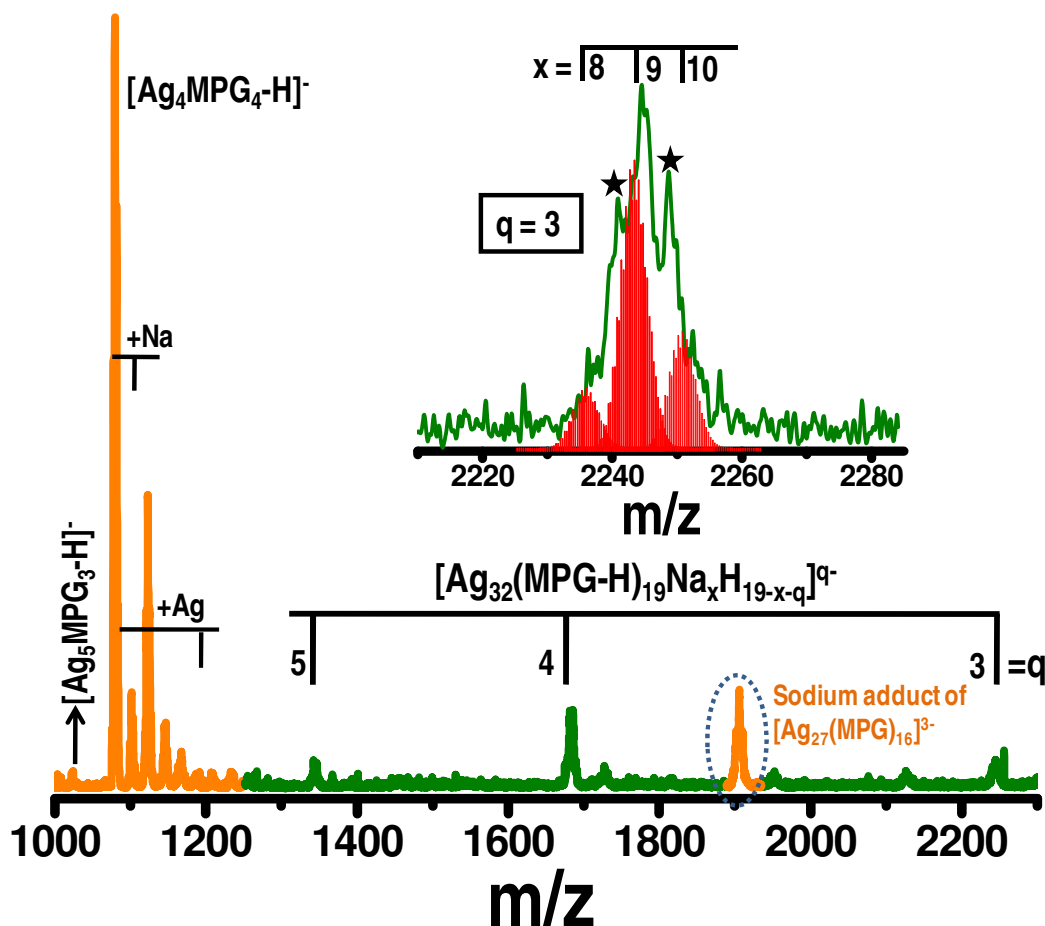


Fig. 5 ESI MS of $\text{Ag}_{32}\text{MPG}_{19}$ in the negative mode in the range of m/z 1000-2300. Calculated positions corresponding to the multiply charged species of $[\text{Ag}_{32}(\text{MPG-H})_{19}\text{Na}_x\text{H}_{19-x-q}]^{q-}$, where $q = 3, 4$ and 5 (shown on the top of the spectrum). Inset shows a comparison of the calculated and experimental spectra of species with $x = 8, 9, 10$ and $q = 3$. These species are $[\text{Ag}_{32}(\text{MPG-H})_{19}\text{Na}_8\text{H}_8]^{3-}$, $[\text{Ag}_{32}(\text{MPG-H})_{19}\text{Na}_9\text{H}_7]^{3-}$ and $[\text{Ag}_{32}(\text{MPG-H})_{19}\text{Na}_{10}\text{H}_6]^{3-}$. The fragments, $[\text{Ag}_{27}(\text{MPG-H})_{16}]^{3-}$ and the Ag thiolates are shown in another color.

The monolayer binding in $\text{Ag}_{32}\text{SG}_{19}$ through thiolate is supported by XPS (Fig. S11†) and FTIR spectroscopy (Fig. S12†). The XPS survey spectrum shows all the expected elements. The Ag 3d peak is close to an Ag(0) value of 368.0 eV. Note that there is not much difference in the

binding energy between Ag(0) and Ag(I) states. The S $2p_{3/2}$ peak is thiolate-like with an observed value of 162.0 eV (Fig. S11c[†]). This is in agreement with the IR spectrum (Fig. S12[†]), which suggests the loss of thiolate proton upon cluster formation. From EDAX, Ag:S atomic ratio measured is $1:0.56\pm 0.03$ which matches with the expected value of 1:0.59 for $\text{Ag}_{32}\text{SG}_{19}$ (Fig. S13[†]). A broad peak centered around $2\theta \approx 38^\circ$ in the X-ray diffraction (XRD) pattern is seen, as in the case of Au or Ag QCs^{17,24,25} which shows the absence of metallic nanoparticles (Fig. S14[†]). The clusters appear as tiny dots in TEM with a size of ~ 1.0 nm (Fig. S15[†]).

A recent breakthrough in metal cluster research is the structure determination of $\text{Au}_{102}\text{SR}_{44}$ followed by those of $\text{Au}_{25}\text{SR}_{18}$ and $\text{Au}_{38}\text{SR}_{24}$. Although the “divide and protect” concept (metal core with neutral atoms protected by metal thiolate) was proposed theoretically by Hakkinen *et al.*⁴⁵ on $\text{Au}_{38}(\text{SR})_{24}$, an understanding of this kind of clusters has taken place only after the above structural data. In $\text{Au}_{102}\text{SR}_{44}$,²² inner core of the cluster contains 79 Au atoms (which are all in neutral state) protected by nineteen $-\text{[RS}_C\text{-Au-S}_C\text{R]-}$ and two $-\text{[RS}_C\text{-Au-S}_B\text{(R)-Au-S}_C\text{R]-}$ units, where $(\text{R})\text{S}_B$ and RS_C correspond to bridging and core-attached thiolates, respectively. $\text{Au}_{38}\text{SR}_{24}$ ²⁰ contains a face-fused biicosahedral Au_{23} core capped by three $-\text{[RS}_C\text{-Au-S}_C\text{R]-}$ and six $-\text{[RS}_C\text{-Au-S}_B\text{(R)-Au-S}_C\text{R]-}$ units. In the case of $\text{Au}_{25}\text{SR}_{18}$, there are two types of ligands, 6 bridging and 12 core-attached thiolates.¹⁹ The whole entity may be represented as $\text{Au}_{13}[\text{RS}_C\text{-Au-S}_B\text{(R)-Au-S}_C\text{R}]_6$. The occupancy of $-\text{[RS}_C\text{-Au-S}_C\text{R]-}$ and $-\text{[RS}_C\text{-Au-S}_B\text{(R)-Au-S}_C\text{R]-}$ in Au_{102} , Au_{38} , Au_{25} is 19:2, 3:6, and 0:6. From these observations, as the size of the core increases to 102, the structure is dominated by $-\text{[RS}_C\text{-Au-S}_C\text{R]-}$ ^{19,22} while in the smaller clusters, $-\text{[RS}_C\text{-Au-S}_B\text{(R)-Au-S}_C\text{R]-}$ units dominate.

Apart from crystal structure studies, NMR can also be used to study the Au-thiolate structure effectively.^{8,46,47} For example, independent NMR studies revealed the presence of two kinds of

sulfur environments in 2:1 ratio (where 2 R_{SC}:1 S_{BR}) in Au₂₅SR₁₈.^{46,48} Motivated by the recent developments and our own earlier studies,⁸ we performed NMR analysis of Ag₃₂SG₁₉. It reveals that the structure of the thiolated cluster is quite different from the phosphine analogue.⁴⁹ The presence of inner core and outer shell with metal thiolate is understood from a detailed analysis of NMR.

¹H NMR data of the cluster are presented in Fig. 6. Chemical shifts for H-3, H-4, H-2, H-9, and H-6 of glutathionate (-SG) in Ag₃₂SG₁₉ are 2.17, 2.60, 3.81, 3.87, and 4.64 ppm, respectively (Fig. 6A, refer to the structure for peak assignments). Protons H-7 (=CH-CH₂-S-) signals are significantly shifted downfield in the range of 3.2-3.5 ppm with broadening followed by splitting, noted as [7, 7] in Fig. 6A. Downfield shift of H-7 can be understood in terms of its close proximity to the silver core. To know the cause of splitting and nature of the staple motif on the cluster surface in comparison to the structures presented above, homonuclear correlation spectroscopy (COSY) and heteronuclear single quantum correlation (HSQC) were performed (Fig. 6B and C, respectively).

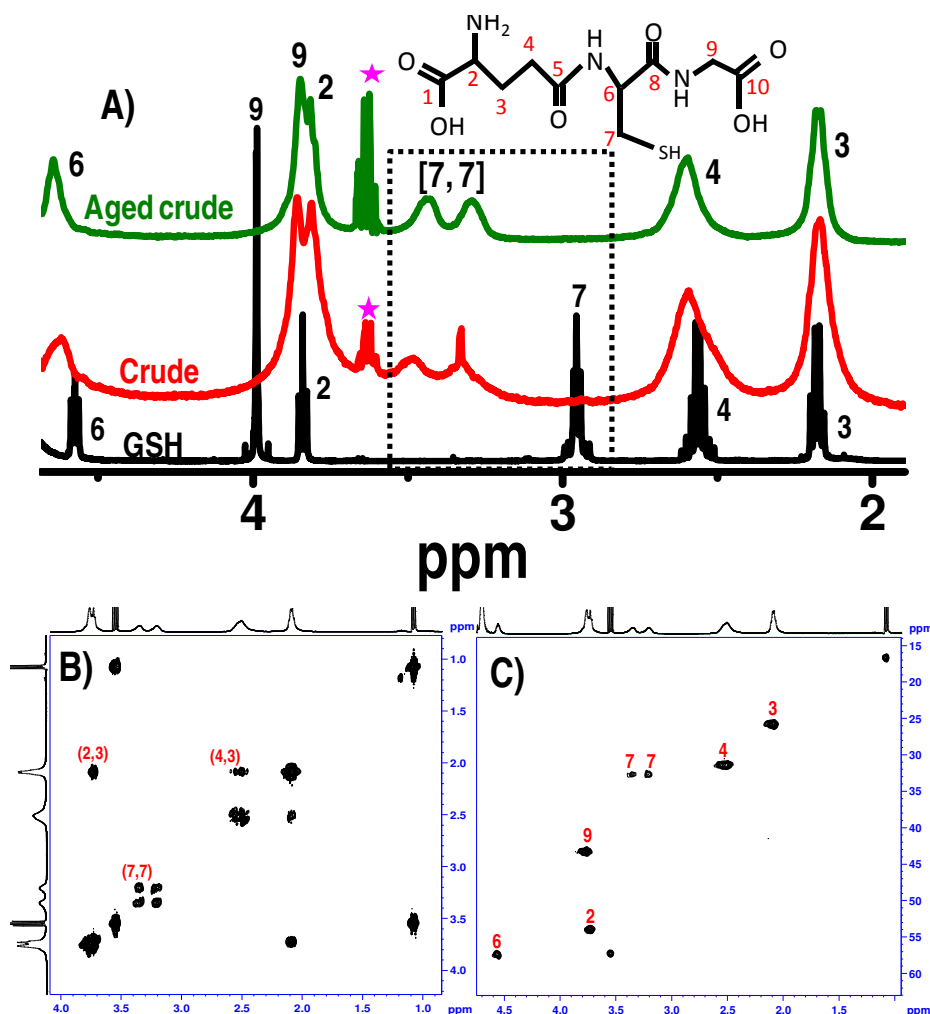


Fig. 6 A) ¹H NMR spectra of GSH, crude cluster and aged crude. The peaks in dotted box are due to H-7. Peaks at ~3.6 ppm (marked with *) are due to residual EtOH. 2D NMR spectra of Ag₃₂SG₁₉ clusters. (B) COSY spectrum. (C) HSQC spectrum. Solvent: D₂O. Note that the CH₃CH₂ signal (¹H: 1.1 and 3.6 ppm, ¹³C: 15.2 and 58.0 ppm) in COSY and HSQC spectrum is from residual CH₃CH₂OH. COSY showed the coupling information from the cross peaks. [4,3] and [2,3] protons are coupled together as understood from their cross peaks, marked in (B). H-7 also produces cross peaks without coupling with other set of protons. In (C), H-7 protons show two signals at 3.2 and 3.5 ppm originating from the same carbon (C-7, 32.0 ppm), due to two hydrogen atoms on C-7.

The two-dimensional (2D) NMR data of Ag₃₂ clearly rules out complete protection of the core by $-\text{[RS}_C\text{-Ag-S}_B\text{(R)-Ag-S}_C\text{R]-}$ units which would have resulted in two pairs of peaks at 2:1 ratio for $-\text{S}_C\text{R}$ and $-\text{S}_B\text{R}$, respectively. It is to be noted that the two peaks in a pair correspond to two hydrogen atoms on the 7th position of glutathione. But, we have seen only one pair of peaks, labeled [7, 7], which are in 1:1 ratio. The presence of 1:1 intensity ratio indicates that all the thiolates are in equivalent environment. Based on the Au-thiolate structure of gold clusters, one can see that $-\text{[S}_C\text{-Ag-S}_C\text{]-}$ staple alone possesses equivalent thiolates. These results suggest that the Ag-thiolate structure for Ag₃₂SG₁₉ is dominated by $-\text{[RS}_C\text{-Ag-S}_C\text{R]-}$. However, complete protection of $-\text{[RS}_C\text{-Ag-S}_C\text{R]-}$ is also not possible due to the presence of odd number of ligands (19 SR). It suggests the presence of other Ag-thiolates. But peaks corresponding to them are not detected in NMR, indicating that they are few in number. From the theoretical study of Xiang *et al.*⁵⁰ and Balasubramanian *et al.*,⁵¹ we know that $-\text{[RS-Ag-RS]-}$ is a stable structural motif for a thiolate-protected Ag QCs. To the best of our knowledge, this is the first experimental evidence for $-\text{[RS-Ag-RS]-}$ structural motif in thiolated Ag QCs. It is in contrast to Au₂₅ and Au₃₈ clusters, where NMR study reveals that they are dominated by $-\text{[RS}_C\text{-Au-S}_B\text{(R)-Au-S}_C\text{R]-}$.

Summary and conclusions

In summary, we have synthesized -SG protected Ag₃₂ clusters. Assignment was made based on ESI MS and MALDI MS experiments. Clusters were characterized with ¹HNMR, 2D NMR, XRD, etc. Cluster with same core was synthesized with MPG as a protecting ligand. ESI MS and MALDI MS also confirm the Ag₃₂MPG₁₉ composition. Based on NMR investigations, we suggest that the most likely the Ag-thiolate is composed of $-\text{[S-Ag-S]-}$ motifs. We believe

that facile synthesis and the structural insights presented here will stimulate further experimental and theoretical studies on this system.

Acknowledgements

We thank the Department of Science and Technology, Government of India for constantly supporting our research program on nanomaterials. M.S.B. thanks the CSIR for a research fellowship.

†*Electronic supplementary information (ESI) available:* Details of experimental procedures and characterization using UV-vis, luminescence, TEM, ESI MS, XPS, FTIR, XRD of Ag₃₂SG₁₉ clusters.

References

1. U. Kreibig and M. Vollmer, J. P. Toennies, Springer, Berlin, 1995.
2. L. M. Liz-Marzán, *Langmuir*, 2005, **22**, 32-41.
3. J. Zheng, P. R. Nicovich and R. M. Dickson, *Annu. Rev. Phys. Chem.*, 2007, **58**, 409-431.
4. R. Jin, *Nanoscale*, 2010, **2**, 343-362.
5. T. G. Schaaff, G. Knight, M. N. Shafiqullin, R. F. Borkman and R. L. Whetten, *The J. Phys. Chem. B*, 1998, **102**, 10643-10646.
6. Y. Negishi, K. Nobusada and T. Tsukuda, *J. Am. Chem. Soc.*, 2005, **127**, 5261-5270.
7. M. A. H. Muhammed, P. K. Verma, S. K. Pal, R. C. A. Kumar, S. Paul, R. V. Omkumar and T. Pradeep, *Chem. Eur. J.*, 2009, **15**, 10110-10120.
8. E. S. Shibu, M. A. H. Muhammed, T. Tsukuda and T. Pradeep, *J. Phys. Chem. C*, 2008, **112**, 12168-12176.
9. E. S. Shibu and T. Pradeep, *Chem. Mater.*, 2011, **23**, 989-999.
10. A. Ghosh, T. Udayabhaskararao and T. Pradeep, *J. Phys. Chem. Lett.*, 2012, **3**, 1997-2002.
11. E. S. Shibu, B. Radha, P. K. Verma, P. Bhyrappa, G. U. Kulkarni, S. K. Pal and T. Pradeep, *ACS Appl. Mater. Interfaces*, 2009, **1**, 2199-2210.
12. R. Jin, H. Qian, Z. Wu, Y. Zhu, M. Zhu, A. Mohanty and N. Garg, *J. Phys. Chem. Lett.*, 2010, **1**, 2903-2910.
13. H. Qian, Y. Zhu and R. Jin, *J. Am. Chem. Soc.*, 2010, **132**, 4583-4585.
14. H. Qian and R. Jin, *Chem. Commun.*, 2011, **47**, 11462-11464.
15. H. Tsunoyama, Y. Negishi and T. Tsukuda, *J. Am. Chem. Soc.*, 2006, **128**, 6036-6037.
16. Z. Wu, M. A. MacDonald, J. Chen, P. Zhang and R. Jin, *J. Am. Chem. Soc.*, 2011, **133**, 9670-9673.
17. M. Zhu, H. Qian and R. Jin, *J. Am. Chem. Soc.*, 2009, **131**, 7220-7221.

18. M. Zhu, C. M. Aikens, F. J. Hollander, G. C. Schatz and R. Jin, *J. Am. Chem. Soc.*, 2008, **130**, 5883.
19. M. W. Heaven, A. Dass, P. S. White, K. M. Holt and R. W. Murray, *J. Am. Chem. Soc.*, 2008, **130**, 3754-3755.
20. H. Qian, W. T. Eckenhoff, Y. Zhu, T. Pintauer and R. Jin, *J. Am. Chem. Soc.*, 2010, **132**, 8280-8281.
21. C. Zeng, H. Qian, T. Li, G. Li, N. L. Rosi, B. Yoon, R. N. Barnett, R. L. Whetten, U. Landman and R. Jin, *Angew. Chem. Int. Ed.*, 2012, **51**, 13114-13118.
22. P. D. Jadzinsky, G. Calero, C. J. Ackerson, D. A. Bushnell and R. D. Kornberg, *Science*, 2007, **318**, 430-433.
23. Z. Wu, E. Lanni, W. Chen, M. E. Bier, D. Ly and R. Jin, *J. Am. Chem. Soc.*, 2009, **131**, 16672-16674.
24. T. Udayabhaskararao and T. Pradeep, *Angew. Chem. Int. Ed.*, 2010, **49**, 3925-3929.
25. T. Udayabhaskararao, B. Nataraju and T. Pradeep, *J. Am. Chem. Soc.*, 2010, **132**, 16304-16307.
26. M. R. Branham, A. D. Douglas, A. J. Mills, J. B. Tracy, P. S. White and R. W. Murray, *Langmuir*, 2006, **22**, 11376-11383.
27. Y. Negishi, R. Arai, Y. Niihori and T. Tsukuda, *Chem. Commun.*, 2011, **47**, 5693-5695.
28. H. Yang, J. Lei, B. Wu, Y. Wang, M. Zhou, A. Xia, L. Zheng and N. Zheng, *Chem. Commun.*, 2013, **49**, 300-302.
29. H. Yang, Y. Wang and N. Zheng, *Nanoscale*, 2013, **5**, 2674-2677.
30. N. Nishida, H. Yao, T. Ueda, A. Sasaki and K. Kimura, *Chem. Mater.*, 2007, **19**, 2831-2841.
31. S. Kumar, M. D. Bolan and T. P. Bigioni, *J. Am. Chem. Soc.*, 2010, **132**, 13141-13143.
32. O. M. Bakr, V. Amendola, C. M. Aikens, W. Wenseleers, R. Li, L. Dal Negro, G. C. Schatz and F. Stellacci, *Angew. Chem. Int. Ed.*, 2009, **48**, 5921-5926.
33. N. Nishida, H. Yao and K. Kimura, *Langmuir*, 2008, **24**, 2759-2766.
34. N. Cathcart, P. Mistry, C. Makra, B. Pietrobon, N. Coombs, M. Jelokhani-Niaraki and V. Kitaev, *Langmuir*, 2009, **25**, 5840-5846.
35. H. Yao, M. Saeki and K. Kimura, *J. Phys. Chem. C*, 2010, **114**, 15909-15915.
36. K. V. Mrudula, T. Udayabhaskararao and T. Pradeep, *J. Mater. Chem.*, 2009, **19**, 4335-4342.
37. N. Cathcart and V. Kitaev, *J. Phys. Chem. C*, 2010, **114**, 16010-16017.
38. I. Diez and R. H. A. Ras, *Nanoscale*, 2011, **3**, 1963-1970.
39. M. Farrag, M. Thämer, M. Tschurl, T. Bürgi and U. Heiz, *J. Phys. Chem. C*, 2012, **116**, 8034-8043.
40. C. Wang, L. Xu, Y. Wang, D. Zhang, X. Shi, F. Dong, K. Yu, Q. Lin and B. Yang, *Chem. Asian J.*, 2012, **7**, 1652-1656.
41. A. K. Singh, R. Kanchanapally, Z. Fan, D. Senapati and P. C. Ray, *Chem. Commun.*, 2012, **48**, 9047-9049.
42. B. Adhikari and A. Banerjee, *Chem. Mater.*, 2010, **22**, 4364-4371.
43. J. Guo, S. Kumar, M. Bolan, A. Desireddy, T. P. Bigioni and W. P. Griffith, *Anal. Chem.*, 2012, **84**, 5304-5308.
44. Z. Wu and R. Jin, *Nano Lett.*, 2010, **10**, 2568-2573.
45. H. Häkkinen, M. Walter and H. Grönbeck, *J. Phys. Chem. B*, 2006, **110**, 9927-9931.
46. Z. Wu, C. Gayathri, R. R. Gil and R. Jin, *J. Am. Chem. Soc.*, 2009, **131**, 6535-6542.

47. H. Qian, M. Zhu, C. Gayathri, R. R. Gil and R. Jin, *ACS Nano*, 2011, **5**, 8935-8942.
48. Z. Wu and R. Jin, *ACS Nano*, 2009, **3**, 2036-2042.
49. G. Schmid, *Chem. Soc. Rev.*, 2008, **37**, 1909-1930.
50. H. Xiang, S.-H. Wei and X. Gong, *J. Am. Chem. Soc.*, 2010, **132**, 7355-7360.
51. Y. Sun, K. Balasubramanian, T. Udayabhaskararao and T. Pradeep, *J. Phys. Chem. C*, 2011, **115**, 20380-20387.

Table of contents

Text: Synthesis and understanding of the staple motif in $\text{Ag}_{32}(\text{SR})_{19}$.

Color graphic:

